

# Chapter 13

## Visualizing Wind Farm Wakes Using SCADA Data

Shawn Martin, Carsten H. Westergaard, and Jonathan White

### 13.1 Introduction

The wind energy used by a turbine to produce electrical power causes a reduction in wind speed behind the turbine, also known as a wake or wind shadow [1]. The wake behind a turbine will dissipate with distance, but will affect nearby downwind turbines. For a large wind farm, these effects will accumulate, resulting in potentially significant aggregate power loss over the entire farm. In addition, wakes are turbulent, and can stress downwind turbines, possibly affecting the reliability and lifetime of turbines within the farm.

To mitigate the effects of turbine wakes in a wind farm, it is important to carefully site turbines during the design phase [1]. Research into siting wind turbines has employed semi-empirical numerical models of turbine wakes [2–5], as well as more exact models based on the Navier–Stokes equations [6]. Power losses due to wake effects have also been modeled [7, 8]. While these models provide valuable insight and guidelines, they are nevertheless incomplete and cannot address every practical concern in the siting of turbines when building a wind farm. Further, there are numerous existing wind farms, for which re-siting is not an option, but which might yield greater power production with improved understanding of on-site wake effects.

An alternative to using computational models for understanding and mitigating wake effects is to analyze data gathered from existing farms using techniques from statistics and data mining. Such approaches have yielded results in the areas of turbine failure prediction and condition monitoring, see, for example, [9–13], but have been applied to lesser degree in wake analysis [14–17].

In this paper, Supervisory Control and Data Acquisition (SCADA) data is analyzed with the goal of documenting wake effects on a functioning industrial scale

---

S. Martin (✉) • C.H. Westergaard • J. White  
Sandia National Laboratories, Albuquerque, NM 87185, USA  
e-mail: [smartin@sandia.gov](mailto:smartin@sandia.gov)

wind farm. SCADA data from this farm is summarized, corrected, transformed, and visualized in order to understand both local turbine–turbine effects and larger wind farm scale effects.

The data is inherently big data, even from only one wind farm, but certainly also if one considers that almost all wind farms daily stream this type of data to data centers around the globe for the owner and operators of wind farms to analyze performance. The primary goal of this paper is to present a novel, holistic visualization of wake effects across a wind farm. This visualization has resulted in the identification of interesting wake type effects such as channel speedup and shear, but it is only a first step in an effort to quantify power loss in existing wind farms due to wake effects. The ultimate goal is not (necessarily) to assist in the layout of new farms, but to validate and potentially improve the performance of existing farms. Once poorly performing turbines and farms are identified, efforts can be made to improve power production. Such efforts would range from preemptively identifying turbines likely to fail (based on their position in a farm and the wake effects acting upon them), to implementing cooperative turbine (smart-farm) strategies. Cooperative strategies work, for example, by directing upwind turbines to operate below peak efficiency so that down wind turbines have additional wind energy available, thereby optimizing aggregate power production [18].

## 13.2 Materials and Methods

*SCADA Data* Data was gathered over a 1.5 year period in 2012 and 2013 from the SCADA system at an onshore wind farm in the USA. The wind farm included 67 horizontal axis, three bladed, variable pitch turbines, along with one meteorological (met) tower. In this study, analysis was performed on a subset of the data collected from the turbines: nacelle wind speed, nacelle direction (position), rotor speed, blade pitch, and power output. The met tower collected data on temperature, air pressure, wind speed, and wind direction. The layout of the wind farm is shown in Fig. 13.1, along with a wind rose showing the prevailing wind directions.

Data was collected continuously (every 2 s) but was summarized over 10 min intervals prior to analysis. For each variable collected (e.g., wind speed), the minimum, maximum, average, and standard deviation over the 10 min interval was computed. After summarization, there were approximately 61,000 time points per turbine available for analysis.

Initial screening required an operational turbine and wind speed to lie in the range of 4–20 m/s, yielding approximately 46,000 time points per turbine, corresponding to a site average wind speed of approximately 8 m/s.

*Met Tower Correction* Due to sensor inaccuracies, various corrections were performed on the wind direction measurements. Following [14], the met tower was considered to have the most accurate wind direction sensor, but was adjusted for systematic bias by comparing the met tower sensor data with data gathered from two nearby turbines, as described next.

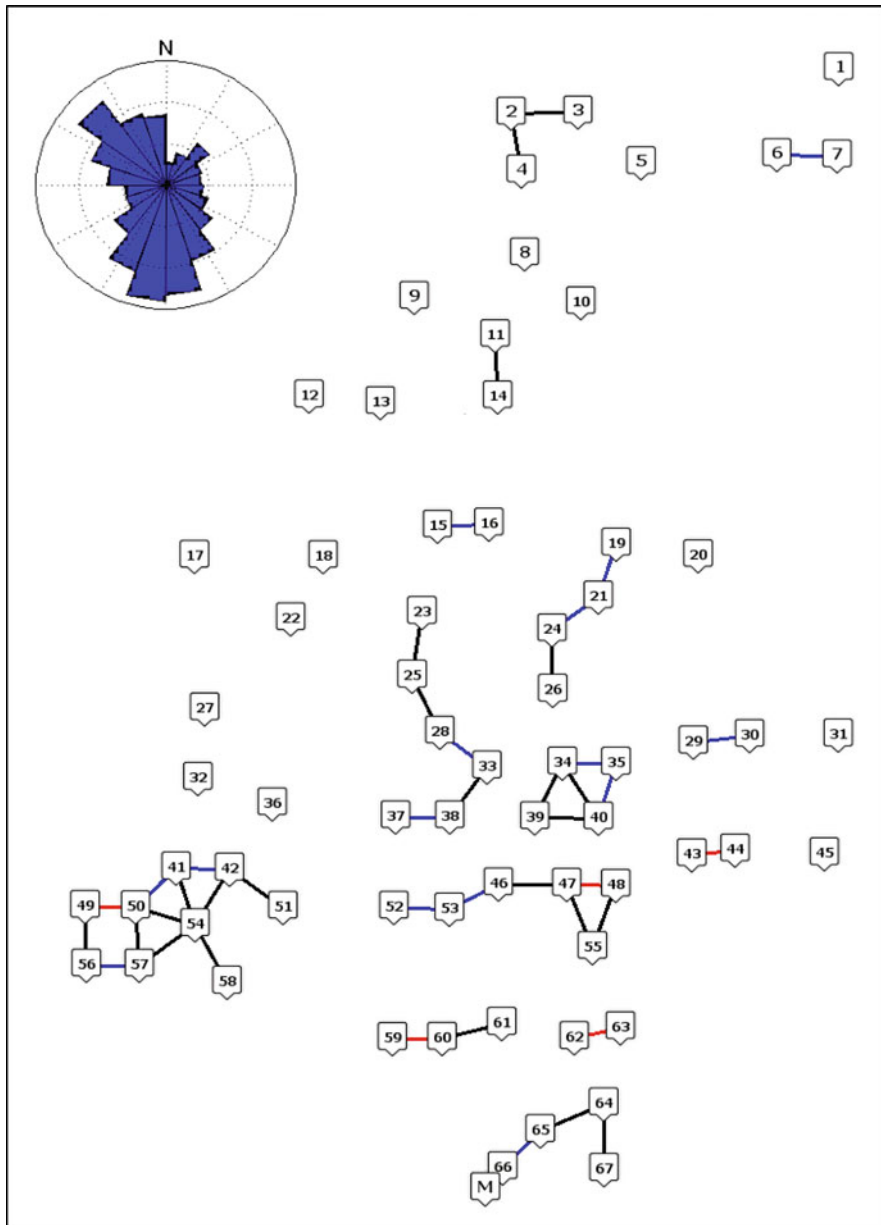


**Fig. 13.1** Wind farm layout. The relative positions of the turbines are shown, with turbines numbered from 1 to 67, and the met tower marked M. The site wind rose is shown in the *upper left*. Turbines in close proximity are connected by lines: turbines within 5 rotor diameters are connected using *red lines*; turbines between 5 and 6 rotor diameters are connected using *blue lines*; and turbines between 6 and 7 rotor diameters are connected using *black lines* (turbines greater than 7 rotor diameters are less likely to experience wake conditions). Icons were taken from the Map Icons Collection (<http://mapicons.nicolasmollet.com>) and are licensed under Creative Commons Attribution (3.0)

Given the measured wind direction at the met tower, denoted  $\theta_m$ , the goal is to find an offset  $\theta_f$  such that

$$\theta_t = \theta_m + \theta_f, \quad (13.1)$$

where  $\theta_t$  is the true wind direction. To find  $\theta_f$ , it is necessary to estimate the true wind direction  $\theta_t$ . Fortunately,  $\theta_t$  can be estimated using the geographical bearing (known exactly) of two turbines near the met tower, and comparing that bearing to the power variability of the downwind turbine. In theory, the power variability of the downwind turbine will peak when the wind direction is exactly aligned with the geographical bearing, providing an estimate of  $\theta_t$ .

The power variability of a turbine is computed as

$$P_v = \frac{\sigma_P}{\mu_P}, \quad (13.2)$$

where  $\mu_P$  is the mean power produced by the turbine, and  $\sigma_P$  is the standard deviation of the power produced, both taken over the 10 min intervals. For the purpose of comparing power variability against wind direction, the power variability is averaged over time for a given wind direction, where the wind directions are binned in  $1^\circ$  intervals.

For the wind farm under investigation, wind direction at the met tower was compared with the power variability of nearby turbine 64. Specifically, power variability was computed for turbine 64 when turbine 64 was downwind from turbine 67. Since turbine 64 is due north (bearing  $180^\circ$ ) of turbine 67, the greatest power variability in turbine 64 should be seen in periods of southerly winds (bearing  $180^\circ$ ). By comparing the power variability of turbine 64 with the wind direction at the met tower, the true wind direction  $\theta_t$  can be estimated, as illustrated in Fig. 13.2. According to this analysis, the measured wind direction  $\theta_m$  was offset from the true wind direction  $\theta_t$  by an angle  $\theta_f \approx 11^\circ$ . The wind rose shown in Fig. 13.1 uses the corrected met mast data.

*Nacelle Direction Correction* The nacelle direction sensors have a number of potential sources of error. First, they are not typically well maintained because the direction is not often used by the turbine controllers. Second, the typically slow changes in yaw and long periods of inaction cause the sensors to experience accuracy loss in relative position. These losses can be jumps in the position or slow deterioration. Although the direction may (in some turbines) be reset by the passage of a switch, some sites have very monotonous wind direction and the turbines rarely trigger the reset. Further, calibration to magnetic North is not always performed, or is sometime re-programmed with turbine software updates. This means that there can be instant jumps in directional determination at discrete times. Finally, if no service records are available, sensors may be replaced, after which absolute direction is lost.

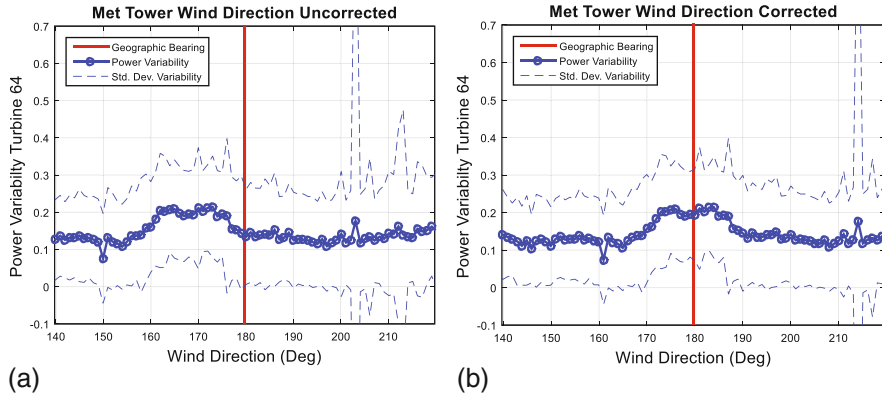


**Fig. 13.2** Met tower wind direction correction. On the left (a), power variability of turbine 64 is plotted against the met mast measured wind direction  $\theta_m$  for winds from the south. A peak in power variability is seen at approximately  $169^\circ$ . In reality, this peak should occur at the geographical bearing from turbine 64 to turbine 67, which is shown as a red line, occurring at  $180^\circ$ . Therefore, the wind direction offset  $\theta_f = \theta_i - \theta_m \approx 11^\circ$ . On the right (b), power variability is plotted against the corrected wind direction, showing an alignment between the peak power variability and the geographic bearing. Throughout this figure, the power variability curves were computed across wind direction bins of  $1^\circ$ . The accuracy of this technique is indicated by the dashed lines in (a) and (b), showing the standard deviation of the power variability

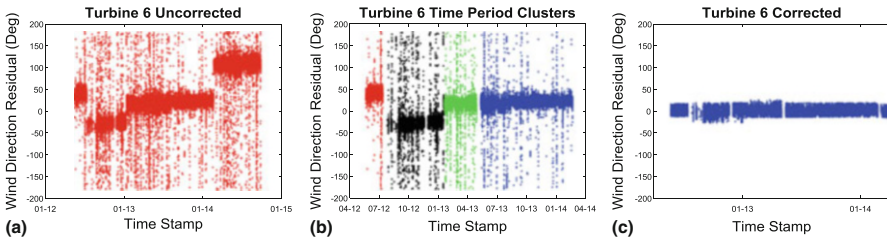


**Fig. 13.3** Nacelle direction correction for turbine 6. On the left (a), the residual wind direction  $\theta_n - \theta_m$  is shown over time for turbine 6, where  $\theta_n$  is the nacelle wind direction and  $\theta_m$  is met tower wind direction. In addition to the additive biases that can be observed, there are several noticeable changes in the measurements at different time points. In the middle (b), the time periods are clustered using a change detection algorithm so that an additive correction can be applied. The separation of the last two groups (green and blue) is due to a period of erratic measurements which can be observed in the uncorrected data as a solid vertical line. On the right (c), additive corrections are applied to the time period clusters and individual measurements significantly different from the mean are removed

The largest obstacle to overcome in correcting the nacelle wind direction is the identification of time period clusters showing significant relative change in wind direction against the corrected met tower data, now considered to be ground truth. An example of this behavior for turbine 6 is shown in Fig. 13.3a. Note that the direction measurements are present only when a turbine is operational and wind speeds exceed 4 m/s, as per the initial data screen.

Each time period cluster is identified using a change detection algorithm [19]. The change detection algorithm proceeds sequentially through each time series searching for time points where the moving average experiences a change beyond a given threshold. For the wind direction measurements, a moving average over 750 time points was used with a threshold of  $20^\circ$ . The results of the change detection algorithm applied to wind direction measurement data from turbine 6 are shown in Fig. 13.3b.

After the time period clusters were identified for a given nacelle, the wind direction based on the nacelle measurements was corrected using additive offsets, as was previously done for the met tower data. Using Eq. (13.1), an offset  $\theta_f$  is applied to the nacelle measurements for each time cluster such that the nacelle wind direction  $\theta_n$  is equal on average to the met tower wind direction  $\theta_m$  for that time period cluster.

Finally, individual wind direction measurements for each nacelle were discarded if greater than one standard deviation from the mean. An example of the corrected data for a nacelle is shown in Fig. 13.3c. The nacelle correction left approximately 34,000 time points per turbine for further analysis.

*Pitch Correction* The final correction compared blade pitch versus wind speed to remove unusual instances of turbine operation. Normally, blade pitch should respond predictably to variations in wind speed, as dictated by the turbine controller. Unusual blade pitch response therefore indicates unusual turbine operation.

To perform this correction, instances of unusual turbine operation were removed if the mean blade pitch was more than one standard deviation from the mean blade pitch schedule, identified empirically by computing mean pitch vs. wind speed, using wind speed bins of 1 m/s. This correction was done on a per turbine basis to account for potential biases in turbine calibration, location, and wind speed measurements. The blade pitch correction for turbine 6 is shown in Fig. 13.4. Pitch correction left approximately 32,000 time points per turbine for further analysis, or approximately 222 days in operation.

*Turbine–Turbine Power Curve Pair Analysis* To motivate the method developed for visualizing wake effects across the entire wind farm, it is instructive to first consider the simpler case of two interacting turbines. For this exercise, consider the relatively isolated pair consisting of turbines 6 and 7, located near the northeast corner of the farm.

Turbines 6 and 7 are close enough (within 6 rotor diameters) that turbine 7 should experience wake effects given a westerly wind. However, wake effects were not observed by plotting the individual power curves for the two turbines, as shown in Fig. 13.5a. Fortunately, this observation is illusory, although the explanation is subtle.

It is important to realize that the wind speed observed by a nacelle is relative to that nacelle. In other words, a downwind nacelle will observe a wind speed slower than the true wind speed, precisely because it is in the wind shadow of the upwind turbine. For the case of two turbines, this problem can be solved by using

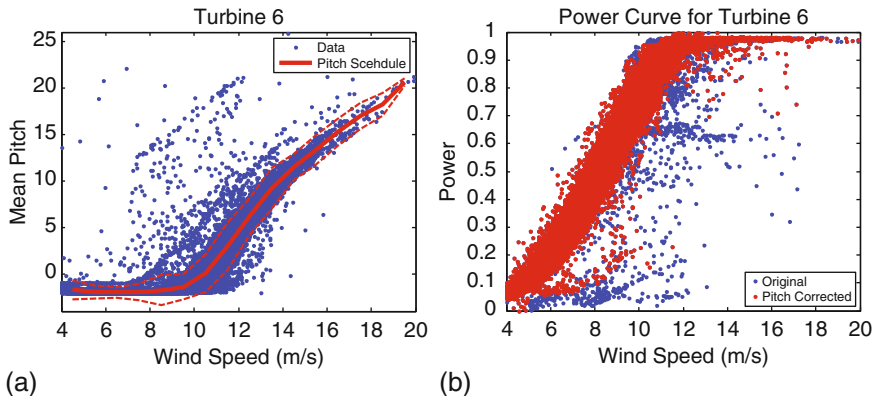


**Fig. 13.4** Pitch correction. On the left (a), the pitch schedule is shown as the variation in mean blade pitch against wind speed. Data points more than one standard deviation from the pitch schedule (indicated by the dashed lines) are removed. On the right (b), the power curve of the corrected data is shown (on a normalized scale). Note that several abnormal operating modes were removed, including de-rated periods. These are seen as blue points below the power curve. The de-rated periods occur in a blue line of points at wind speeds from 10 to 14 m/s and power level at  $\sim 0.65$

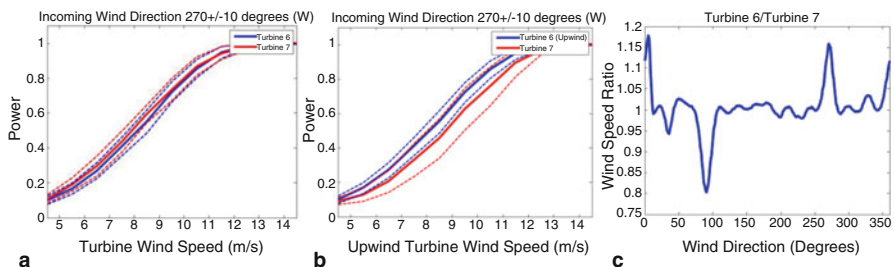


**Fig. 13.5** Wake effect for turbine 7. On the left (a), power curves are shown for the upwind turbine 6 and the downwind turbine 7 (given westerly winds). These curves were obtained by averaging the nacelle power measurements over bins with width of 1 m/s, and the dotted lines denote 1 standard deviation from the mean. The curves show no wake effect because the individual nacelle wind speed measurements were used on the x-axis. In other words, both turbines are functioning normally according to the wind speeds they are observing. In the middle (b), power curves are shown for the same two turbines, this time using the upwind nacelle (turbine 6) sensor to measure wind speed on the x-axis. These curves show a wake effect, because turbine 7 is under-performing relative to turbine 6, given the wind speed it would observe if it were not in the wake of turbine 6. On the right (c), the ratio of the wind speed from turbine 6 to turbine 7 is plotted versus wind direction. The wind speeds were binned as described in the text for the normalized instant power plots. The wake effect between turbines 6 and 7 for westerly winds is observed as a peak at  $270^\circ$  and for easterly winds as a trough at  $90^\circ$  (the peak at  $0^\circ$  is due to the fact that turbine 7 is in the shadow of turbine 1 for northerly winds)

the upwind turbine wind speed measurement as the true wind speed, as shown in Fig. 13.5b. Alternatively, the ratio of the nacelle wind speeds can be plotted versus wind direction, as shown in Fig. 13.5c.

Unfortunately, the solutions used for turbines 6 and 7 will not scale to the entire wind farm, as they are both still relative measures. In other words, which turbine should be used to provide the baseline wind speed measurement? Imagine, for example, a row of turbines in line with the wind. The only turbine that is not in a wind shadow is the leading turbine. Thus the leading turbine will report the true wind speed, while every other turbine will report a wind speed slower than the true wind speed. The last turbine in the row will report the slowest wind speed. Which turbine should be used to measure the true wind speed? Which wind speed ratios should be used to visualize the wake effects? This situation is of course further complicated in an array of turbines, or as in the case of an actual farm, an irregular distribution of turbines.

*Directional Power Performance and Variance Plots* The previous discussion of nacelle wind speeds suggests a new approach for visualizing wake effects: use an average measurement over the entire farm as a baseline in order to compare individual turbines. Since wind speed and power are intimately related for a turbine, and since the power measurements were more accurate in the dataset under consideration, a normalized measure of instantaneous power was employed. For turbine  $i$ , the *normalized instant power* is defined to be

$$P_N(t) = P_i(t)/\mu_{P(t)}, \quad (13.3)$$

where  $P_i(t)$  is the power of turbine  $i$  over the 10-min interval  $t$ , and  $\mu_{P(t)}$  is the average power over all turbines over the same interval. For example, if turbines 6 and 7 made up the entire wind farm, then the normalized instant power of turbine 6 would be  $P_N(t) = 2P_6(t)/(P_6(t) + P_7(t))$ . The normalized instant power avoids the use of wind speed measurements and can also be averaged over time and binned against wind direction to obtain polar plots showing the performance of a given turbine against the performance of the wind farm as a whole. For the normalized instant power plots, bins centered at every integral degree (e.g.,  $0^\circ$ ,  $1^\circ$ , ...,  $359^\circ$ ) were used. These bins were overlapping and covered sectors  $16^\circ$  wide (e.g.,  $[-8^\circ, 8^\circ]$ ,  $[-7^\circ, 9^\circ]$ , ...,  $[351^\circ, 7^\circ]$ ). The main reason to use overlapping bins was to smooth the resulting plots, due to a lack of data in certain wind directions. The  $16^\circ$  sectors correspond to anticipated wake effects for turbines separated by 7 rotor diameters. An example of normalized instant power plots, again assuming turbines 6 and 7 make up the entire wind farm, is shown in Fig. 13.6. (Note the similarities of the normalized instant power plots with the plot of relative wind direction in Fig. 13.5c.)

In Fig. 13.6, the mutual wakening of the two turbines at  $90^\circ$  and  $270^\circ$  can be clearly observed. For turbine 6, there is a hint of wake deficit from turbine 1 at  $30^\circ$  and a stronger deficit bearing  $0^\circ$  for turbine 7. The difference in the deficit is smaller at turbine 6 due to the larger distance to turbine 1. Turbine 7 also shows an apparent

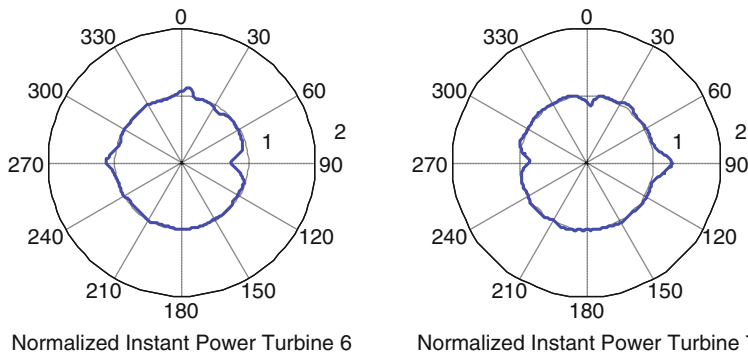


**Fig. 13.6** Normalized instant power plots. These plots show normalized instant power (see Eq. 13.3) averages over time versus wind direction for turbines 6 and 7. The plots are arranged to mirror the positions of the turbines in the wind farm, so that turbine 6 is west of turbine 7. Thus, given a westerly wind, turbine 6 is upwind and turbine 7 is downwind. In this case, turbine 7 is under-performing relative to turbine 6, so that a dip is observed in the plot for turbine 7 at the angle  $270^\circ$  (and a corresponding bump is seen for turbine 6 at  $270^\circ$ ). There are also bumps and dips at  $90^\circ$ , and the bump in turbine 6 at  $0^\circ$  and corresponding dip in turbine 7 occur because of the wake from turbine 1 just north of turbine 7. Both plots are obtained by averaging normalized instant power over time using wind direction bins  $1^\circ$  apart

increase at  $90^\circ$ . Note that these plots are slightly different from the plots generated for the entire wind farm (Fig. 13.8), since this example is normalized against only turbines 6 and 7 (i.e., this example assumes the wind farm consists only of turbines 6 and 7, even though the other turbines in the farm clearly affect the turbine 6 and 7 subset).

A variation on the normalized instant power computation is power variability, as defined in Eq. 13.2. Power variability averages over time can be computed and binned against wind direction (again using overlapping bins  $1^\circ$  apart covering  $\pm 8^\circ$  sectors) as shown in Fig. 13.7.

*Colored Polar Plots* The normalized instant power and power variability polar plots can be used to visualize wake effects across an entire wind farm. To facilitate viewing multiple plots simultaneously, a color scale can be added to the plots. For the instant power visualization these colors highlight over-/under-performing turbines, and for the power variability visualization the colors highlight high/low power variance per turbine. The color scales are computed to be comparable across the entire farm (i.e., the same scale is used for every plot in the entire visualization). Visualizations of the wind farm are given in Fig. 13.8. Wake effects are easily seen using these images.

Note that the average power in the normalized power computation is taken over periods where most of the farm is operational, but not necessarily the entire farm. Specifically, average power is computed when at least 62 turbines are operational, or no more than 5 turbines are not operating. This measure avoids ignoring periods

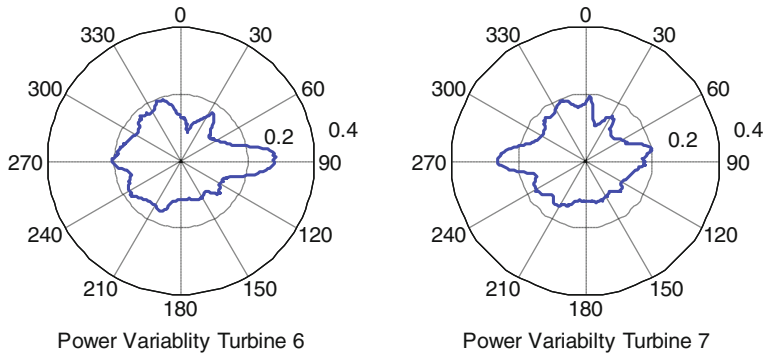


**Fig. 13.7** Power variability plots. These plots show power variability (see Eq. 13.2) over time against wind direction for turbines 6 and 7. They are again arranged to mirror the positions of the turbines in the wind farm. Wake effects can be observed as increased variability, which manifest as bumps on the plots. Thus there are bumps at  $90^\circ$  (easterly wind) for turbine 6 and  $270^\circ$  (westerly wind) for turbine 7. Both plots are obtained by averaging power variability over time using wind direction bins  $1^\circ$  apart

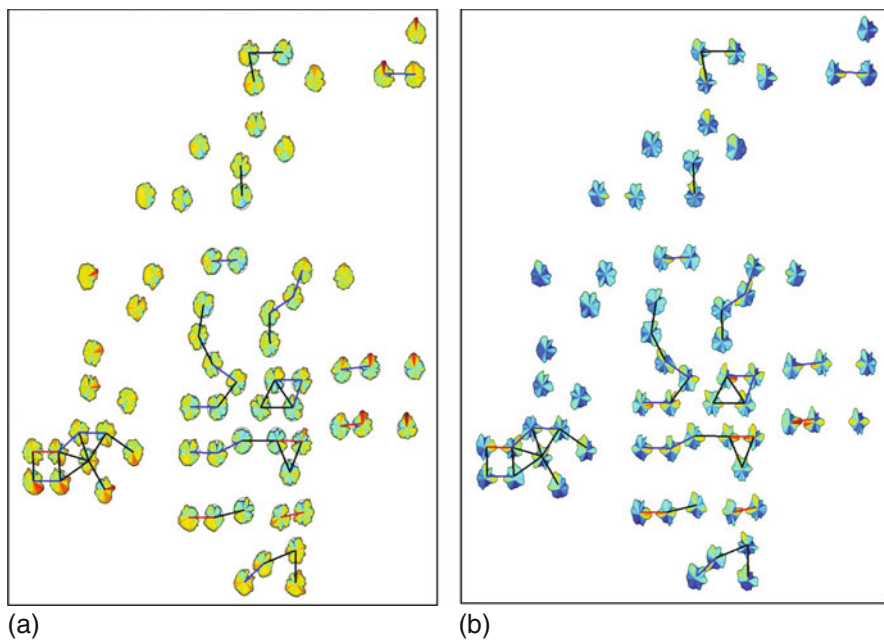


**Fig. 13.8** Wake effect visualizations. On the left (a), visualization is shown using normalized instant power, and on the right (b), visualization is shown using power variability. In both cases, the rose plots are positioned in place of the number icons seen in Fig. 13.1. Further, the rose plots are colored according to the radial magnitude. For the instant power plots, over-performing turbine directions are colored red, while under-performing turbine directions are colored blue. Grey circles show average performance (instant normal power value of 1). For the power variability plots, high variability directions are colored red, and low variability directions are colored blue

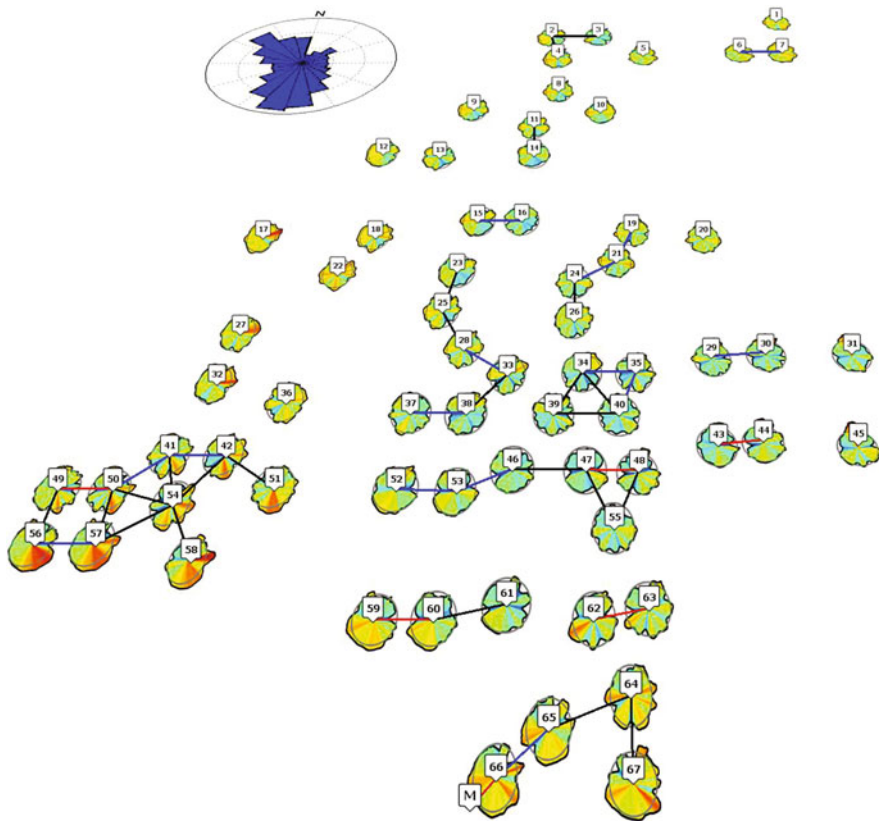


**Fig. 13.9** Google Earth visualization. This visualization shows the wind farm wake effects using the normalized instant power plots, complete with the labels from Fig. 13.1. Grey circles show average performance (instant normal power value of 1). The wind farm terrain imagery (not shown) can also be examined for correlations between performance and local topography

when the farm is operational except for a few down turbines (or turbines with previously discarded measurements).

The visualization can also be displayed using Google Earth (<http://www.google.com/earth>) for improved interactivity. An example of a fully interactive visualization is shown in Fig. 13.9.

### 13.3 Results

In this section, a more detailed analysis of the wind farm is provided, using the normalized instant power and power variability plots, as well as other simpler curves. To start, it is interesting to understand the overall performance of the farm in relation to wind direction. Although it is not useful to take the average of the

normalized instant power plots (since they are normalized they average to 1), it is useful to consider the average turbine power relative to wind direction, as shown in Fig. 13.10a. As expected, this plot is highly correlated with the wind rose for the site, albeit with an unusual spike in production from the E-SE. The power variability plots, unlike the instant normalized power plots, can be averaged, since they are computed independently per turbine. The power variability averages over the wind farm is shown in Fig. 13.10b. There are three large lobes of variability at  $90^\circ$ ,  $270^\circ$ , and  $340^\circ$ . The lobes at  $90^\circ$  and  $270^\circ$  are most likely associated with turbulence generated by closely positioned E-W turbine pairs, as there are a significant number of turbines in the  $90 - 270^\circ$  neighboring direction. This can be seen comparing the turbine to turbine bearing, as shown in Fig. 13.10c, to the variance distribution. The high variance at  $340^\circ$  is aligned with the main wind direction, and a large nearby wind farm to the NW. There is less variation along the other main wind direction to the SSE, but the neighboring wind farms in this direction are further away and shadow only the east part of the farm.

In Fig. 13.8 it is also apparent that individual turbine performance and variation is related to position within the wind farm, where turbines towards the center of the farm have lower performance and higher variability. This is more easily visualized by averaging the normalized instant power and power variability plots over all wind directions, as shown in Fig. 13.11.

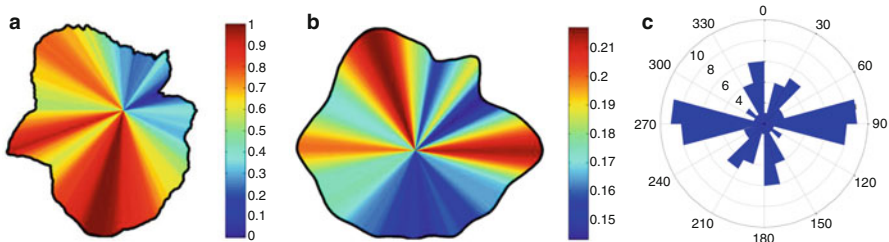


**Fig. 13.10** Overall wind farm performance. On the left (a), the power averaged over all turbines versus wind direction is shown, maximum normalized to 1. As expected, this polar plot is highly correlated with prevailing wind directions (NW and S), although there is also an interesting spike in the E-SE direction. In the middle (b), the average power variability versus wind direction is shown. The power variability is stretched N-S with prevailing winds and E-W by a large number of closely positioned E-W turbine pairs. On the right (c), a radial histogram of counts for turbine-turbine pairs within 7 rotor diameters is shown (turbines farther than 7 rotor diameters are less likely to experience wake conditions)

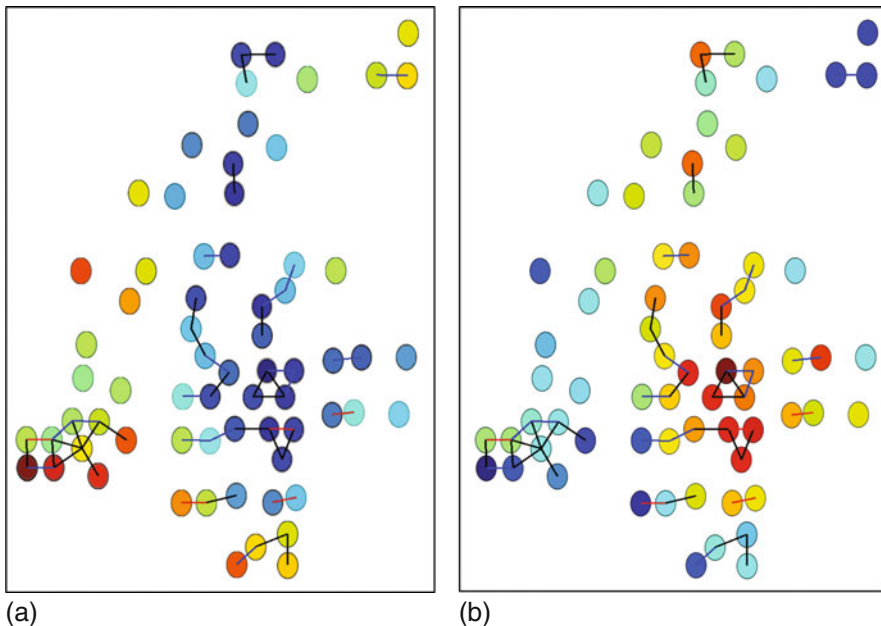


**Fig. 13.11** Average turbine performance over wind farm. On the left (a), the wind direction averaged normalized instant power is shown for each turbine, where red indicates high performance, and blue indicates low performance. On the right (b), the wind direction averaged power variability is shown for each turbine, where red indicates high variability, and blue indicates low variability

*Detailed Wake Analysis* In addition to providing an overview of the wind farm, the normalized power and power variability plots can be used to understand wake effects on a more detailed scale. Four distinct features have been observed in the data:

- wake deficit effects,
- speedup channels from two upstream turbines,
- shear point speedup from one upstream turbine, and
- shear point speedup from multiple upstream turbines or an upstream farm.

Wakes are characterized by a power deficit in the direction of a neighboring turbine and a distinct increase in power variance. In Fig. 13.12, two distinct wake effects can be seen at turbine 11, originating from turbines 8 and 10. The first effect is the wake deficits, seen as dips in the normalized power plot of turbine 11 facing turbines 8 and 10, as well as peaks in the power variability.

The second observed effect is a speedup when a turbine is facing the midpoint of two upwind turbines. Here the power is higher than average, also seen in Fig. 13.12 when turbine 11 is facing the midpoint between turbines 8 and 10. This effect is

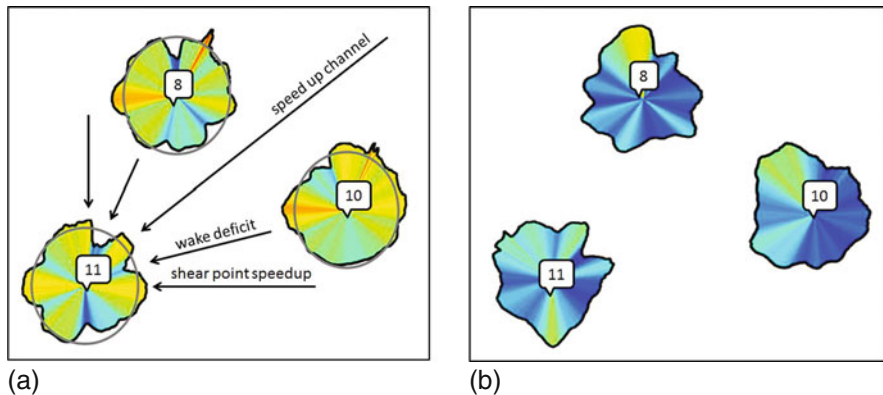


**Fig. 13.12** Wake effects. On the left (a), three wake effects can be observed using instant normalized power plots for turbines 8, 10, and 11. Wake deficits can be seen as dips in the power production when turbine 11 is in the shadow of turbines 8 or 10; a speedup channel can be seen as a peak in the power production when turbine 11 is facing the midpoint of turbines 8 and 10; and shear point speedups can be seen when turbine 11 is tangent to the wake of turbine 10 or 8. On the right (b), the corresponding variability in power is shown

generally not included in the standard wind farm modeling tools, even though it is apparently significant. Somewhat surprising, the power variance in this direction is significantly lower than average.

A third effect occurs when the upstream wake is barely touching the downstream turbine, causing an increase in power. This occurs in Fig. 13.12, for example, when increased power is observed at turbine 11 just south of the downstream sector of turbine 10. Surprisingly, this is also associated with a low variance. We call this effect *shear point speedup*.

Both types of speedup effects seem to be amplified in cases of multiple upstream turbines and even a whole upstream wind farm. Finally, the three effects are also observed as products of the landscape, i.e., clusters of trees or buildings (data not shown).

**Aggregate Wake Deficit** The wake deficit is straightforward to detect when the wake is produced by a single upstream turbine which is relatively undisturbed. In this case, the power variance has a very clear peak in the direction of the upstream turbine, and the power produced has a corresponding minimum. Additional discussion using wake profiles to illustrate these observations is provided in the Appendix.

In a multi-turbine wake situation, however, detecting wake effects is more difficult. Nevertheless, a generic wake deficit effect can be observed across the entire wind farm. To see this effect, 854 turbine pairs were selected within 25 rotor diameters and an undistributed direct path between them (to observe potential wake effects). From these pairs, the minimum power deficit and maximum variance of the downwind turbine were recorded. These values are shown in Fig. 13.13 versus

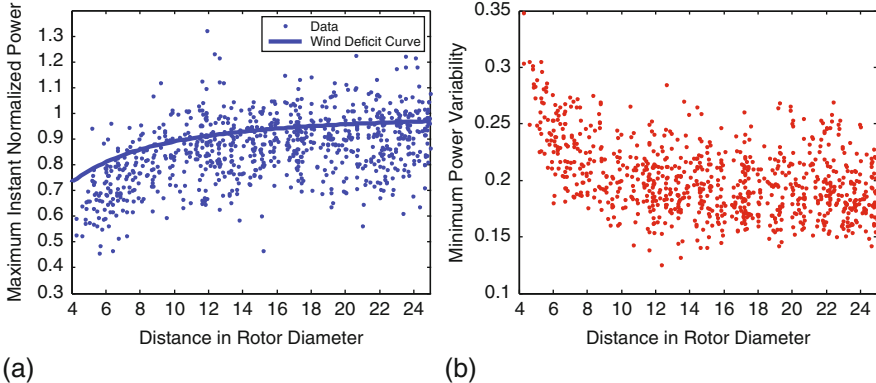


**Fig. 13.13** Power deficit versus distance. Maximum instant normalized power and minimum power variance for a downstream turbine were collected for 854 turbine pairs. On the left (a), the maximum normalized instant power is plotted versus distance behind the upwind turbine. The semi-empirical wind velocity deficit from Eq. (13.4) is shown as a *solid curve*. On the right (b), the minimum power variance for the downstream turbine versus distance is shown

distance between turbine pairs. For the normalized instant power in Fig. 13.13a, the semi-empirical expression for wind velocity deficit described by Katic et al. [4] is also shown. This expression is given as

$$\frac{U_x}{U_0} = 1 - \frac{1 - \sqrt{1 - C_T}}{(1 + 2k_D^x)^2}, \quad (13.4)$$

where  $U_0$  is the upstream wind velocity,  $U_x$  is the wind downstream velocity at a distance  $x$  behind the turbine,  $C_T$  is the coefficient of thrust, and  $k$  is an empirical decay constant, given as 0.075 or 0.11 [4]. Reasoning that annual energy production is typically quasi-linear with wind speed averaged over time, the wind velocity deficit is compared with the normalized instant power in Fig. 13.13a to surprisingly good effect. For the wind velocity deficit,  $k$  was taken to be 0.075 and  $C_T$  was set to 0.9.

*Channel Speedup Profiles* It has been observed from the normalized instant power plots that there is a significant performance improvement when a turbine is facing the midpoint between two upwind turbines. The physical explanation could be that the wakes of the two upstream turbines displace airflow, which accelerates as in an ordinary channel contraction. Even minor speedup effects would boost the performance of the downstream turbine. For cases discussed in the Appendix, the boost is between 1.1 and 1.3 times average. The profiles also display a wake deficit next to the peak, as the downstream turbine faces either one of the two upstream turbines (see Figs. 13.16 and 13.17 in the Appendix).

Two turbines (17 and 58) show an excessive over performance (1.4–1.5 times average) facing what could be described as a duct or channel from the East, formed by rows of multiple neighboring turbines (these turbine profiles are not plotted). See Fig. 13.9.

Channel speedups exhibit a lower variance than the average of the farm, as might be expected from multiple upstream turbines. This could be explained by the two upstream wakes displacing each other away from the downstream turbine, thus reducing wake turbulence. Further, if there is a speedup effect in a channel type arrangement, turbulence will generally be suppressed due to contraction.

*Shear Point Speedup Profiles* For shear point speedup, the upstream obstacle, in this case a turbine wake, forces the incoming wind to go around and thus speedup along the side of the farm. This is seen as increased power in the downstream turbine. The shear point speedup effect is investigated for seven turbines, shown in Figs. 13.18 and 13.19 in the Appendix. Within the dataset, the increase occurs  $15^\circ$  to  $20^\circ$  from the bearing of the upstream turbine, with a magnitude of 1.1–1.22 times the average farm level. This magnitude is less than the speedup channel effect, but still significant. Again, this effect is associated with a wake presence. Effects like these have been observed in connection with buildings upstream to wind turbines, (see, e.g., Corscadden et al. [20]). Building speedup is also seen in this dataset (for example, turbine 7, bearing  $80^\circ$ ), but is not investigated further.

*Shear Speedup for Multiple Upstream Turbines* Turbines 1, 6, 30, 31, 44, and 45 exhibit a narrow and a very high increased performance peak close to due north. This is due to a displacement from multiple upstream turbines. Turbines 1 and 6 face a long row of turbines in an upstream wind farm at approximately  $15^\circ$ . The  $15^\circ$  angle is comparable to what is observed for the shear point speedup from a single turbine. Several other turbines, for example, 7, 20, 29, and 43, also show the speedup, but the wake profiles are masked by a combination of speedup and waking. The wake profiles for these turbines are shown in Figs. 13.20 and 13.21 of the Appendix.

## 13.4 Conclusions

Based on a directional power performance analysis, four wake effects inside a 67 turbine wind farm have been identified. These effects include traditional wind shadows, channel speed ups, and shear effects. The analysis shows that a directional decomposition of turbine performance within the farm provides a holistic view of wind farm performance that can reveal more subtle features than standard power curve analysis. Further, the analysis can be made relative to subsets of the turbines in the wind farm (by normalizing against the smaller group), to highlight more subtle effects in performance. The results have been obtained even though the wind speeds have been almost completely ignored in the analysis.

Data preparation and validation was performed prior to analysis. The scrubbing of the data for sensor calibration errors and abnormal operational situations were the two most important issues [14, 22]. Furthermore, automatic processing was needed. The data analysis accurately corrected the turbine yaw position.

The wake losses identified are in reasonable agreement with classical models for wake losses. Comparing the observations to existing wake models, these only take into account the wake losses (i.e., recovery to nominal wind speed), but do not include the upside from speedup effects, due to channel or shearing points that have been observed. These new discoveries seem to be absent from the existing knowledge base and are necessary to understand in order to improve wind farm performance. Of course, these effects may be illusory and a side effect of our data analysis. Further investigation in terms of more detailed computational simulations, or suitable experiments would be necessary to provide definite evidence either way.

The suppressed variability of the speed up effect could be affecting turbine loading and reliability in a positive way, opposite the manner in which increased variability is known to have an adverse effect. Future correlation of turbine failures with directional observance could improve the understanding of wind farm operations with respect to reliability.

In the analysis, individual wake profiles and speedup effects were clearly identified. An individual turbine's average yearly operational situation is complex: even small wind direction changes can have large effects. Wakes were analyzed against nearest neighbors, but in the future, a multi-wake analysis could be extracted from the data as well, possibly using a superposition principle similar to those applied in classic wind farm models [2–4]. It may also be desirable to analyze additional data and explore different wake states based on power performance, i.e., restrict to region III rotor thrust of the power curve and analyze wind farms near nominal power, as was seen in Horns Rev data [21].

This work is a first step towards quantifying power production loss and impact on reliability of wind farm wake effects in existing wind farms. The ultimate goal of the work is not (necessarily) to assist siting new farms, but to improve the performance of existing farms. Once poorly performing turbines and farms can be accurately identified, efforts can be made to improve power production. Such efforts would range from pre-emptively identifying turbines likely to fail (based on their position in a farm and the wake effects acting upon them), to implementing cooperative turbine (smart-farm) strategies [18].

**Acknowledgements** This work is supported and made possible by the Department of Energy (DOE) Wind and Water Power Program. Sandia National Laboratories is a multi-program laboratory managed and operated by Sandia Corporation, a wholly owned subsidiary of Lockheed Martin Corporation, for the US Department of Energy's National Nuclear Security Administration under contract DE-AC04-94AL85000. Wind farm SCADA data was provided by a strategic industrial partner.

## Appendix

### *Abstract*

This Appendix provides additional analysis regarding the four wake effects discussed in the results section of the paper “Visualizing Wind Farm Wakes Using SCADA Data.” The four effects observed are

- wake deficit effects,
- speedup channels from two upstream turbines,
- shear point speedup from one upstream turbine, and
- shear point speedup from multiple upstream turbines or an upstream farm.

For the purposes of continuity, some of the text from the paper is repeated.

### ***Wake Deficit Profiles***

To illustrate the four wake effects observed using the instant power and power variability plots, profiles for various turbines are shown. The wake deficit, for example, is straightforward to detect when the wake is produced by a single undisturbed upstream turbine. In this case, the power variance has a very clear peak in the direction of the upstream turbine, and the power produced has a corresponding minimum. Wake profiles showing wake deficits for 10 turbines pairs in terms of normalized instant power are shown in Fig. 13.14, with the corresponding power variance profiles shown in Fig. 13.15.

The detection of a wake deficit is straightforward when the wake is produced by a single undisturbed upstream turbine. In particular, the power variance signature is a very clear peak in the direction of the upstream turbines. However, in a multi-turbine wake situation, detecting wake effects is more difficult. For example, turbine 62 waked by turbine 63 shows a clear wake deficit and an increased variance, but has two distinct side lobes where the power increases over the average value outside the core of the wake. This is most likely due to wakes upstream of turbine 63 in an adjacent upstream wind farm. It is also interesting to observe that the peak variance is exactly pointing towards turbine 63, but the wake deficit is a few degrees off to the left. Turbine 10 waked by turbine 11 exhibits the opposite behavior, where the wake is symmetric, but the variance profile is asymmetric. In general, however, the variance profiles are symmetric.

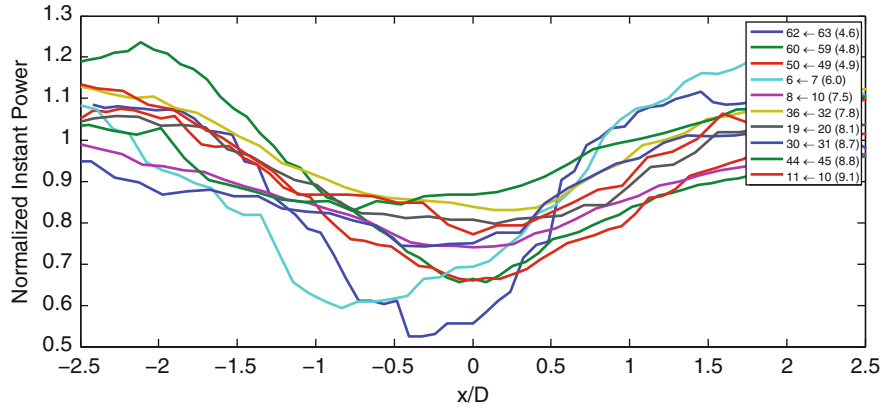


**Fig. 13.14** Normalized instant power for waked turbines. The  $x$ -axis gives the wind direction degree offset normalized by the distance between the turbines (e.g.,  $x/D = \theta^\circ \left( \frac{\pi}{180^\circ} \right) \left( \frac{x}{D} \right)$ , where  $\theta^\circ$  is the offset in degrees,  $x$  is the distance between the two turbines, and  $D$  is the rotor diameter). For example, when the offset is  $0^\circ$  the wind is blowing straight from the upwind to the downwind turbine. The  $y$ -axis shows the normalized instant power for the downwind turbine. The turbine pairs selected are given in the legend, where the notation  $d \leftarrow u$  ( $r$ ) indicates the downwind turbine ( $d$ ), the upwind turbine ( $u$ ), and the distance ( $r$ ) in rotor diameters. See also Fig. 13.1 for turbine positions

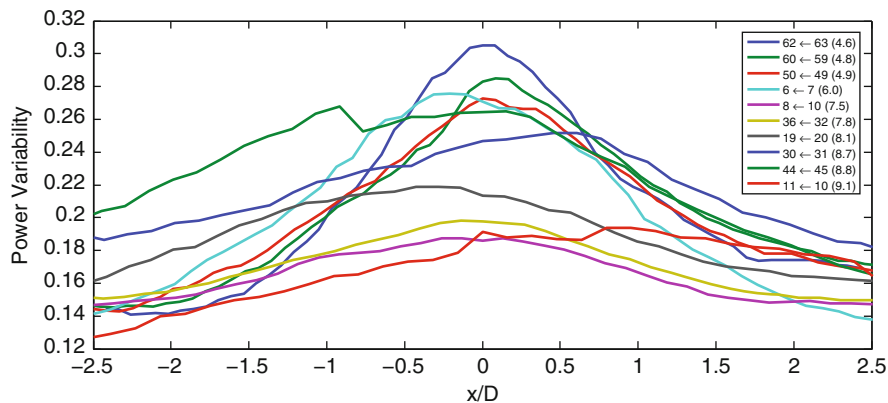


**Fig. 13.15** Power variability for waked turbines. As in Fig. 13.14, the  $x$ -axis gives the normalized wind direction degree offset from the upwind turbine. The  $y$ -axis gives the power variability of the downwind turbine

## Channel Speedup Profiles

It has been observed from the normalized instant power plots that there is a significant performance improvement when a turbine is facing the midpoint between two upwind turbines. The physical explanation could be that the wakes of the two upstream turbines displace airflow, which accelerates as in an ordinary channel contraction. Even minor speedup effects would boost the performance of the downstream turbine. For the selected profiles in Fig. 13.16, the boost is between 1.1 and 1.3 times average. The profiles also display a wake deficit next to the peak, as the downstream turbine faces either one of the two upstream turbines.

Channel speedups exhibit a lower variance than the average of the farm, as seen in Fig. 13.17, which might be expected from multiple upstream turbines. This could be explained by the two upstream wakes displacing each other away from the downstream turbine, thus reducing wake turbulence. Further, if there is a speedup effect in a channel type arrangement, turbulence will generally be suppressed due to contraction.

## Shear Point Speedup Profiles

For shear point speedup, the upstream obstacle, in this case a turbine wake, forces the incoming wind to go around and thus speedup along the side of the farm. This is seen as increased power in the downstream turbine. The shear point speedup effect is investigated for seven turbines, shown in Figs. 13.18 and 13.19. Within the dataset,

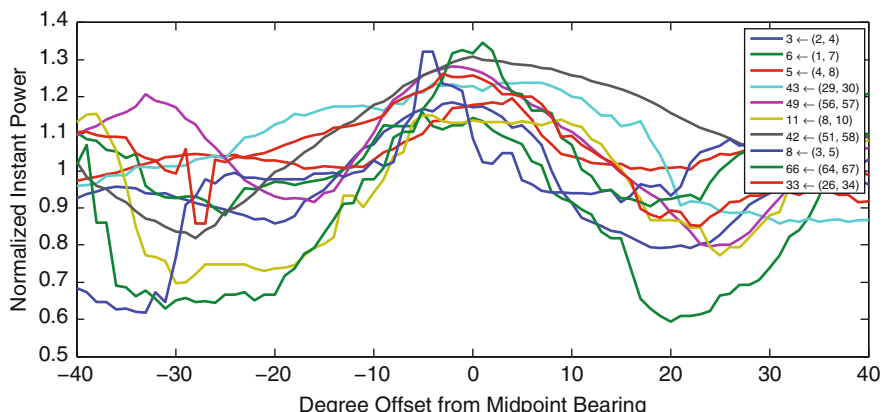


**Fig. 13.16** Normalized instant power for channel speedup. The  $x$ -axis gives the wind direction degree difference from the downstream turbine to the midpoint between the two upstream turbines. The  $y$ -axis gives the normalized instant power. The channel speedup effect can be seen as the peak at  $0^\circ$ , flanked by wake deficits on either side of the peak

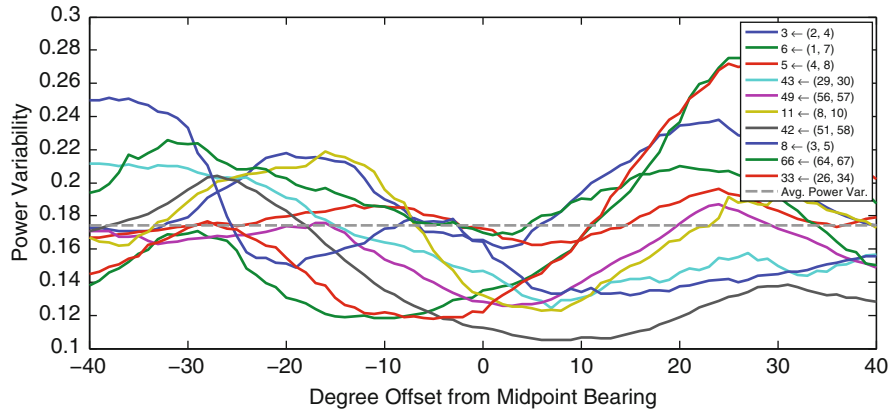


**Fig. 13.17** Power variability for channel speedup. As in Fig. 13.16, the  $x$ -axis gives the wind offset from the midpoint between the two upstream turbines. The  $y$ -axis gives the power variability. The channel speedup is associated with low variability, as compared to the average variability over the farm, shown as a gray dashed line

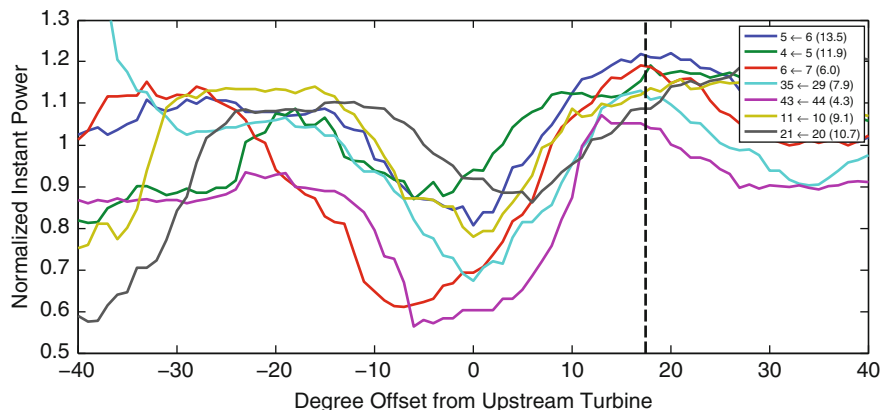


**Fig. 13.18** Normalized instant power for shear speedup. The  $x$ -axis gives the wind direction degree offset from the bearing between the upwind and downwind turbine pair, and the  $y$ -axis shows the normalized instant power. Turbines were selected so that the region between  $0^\circ$  to  $90^\circ$  from the downwind turbine is undisturbed (no turbines nearby). The shear point speedup can be seen as improved power production between  $15^\circ$  and  $20^\circ$ , as indicated by the dotted line at  $17.5^\circ$

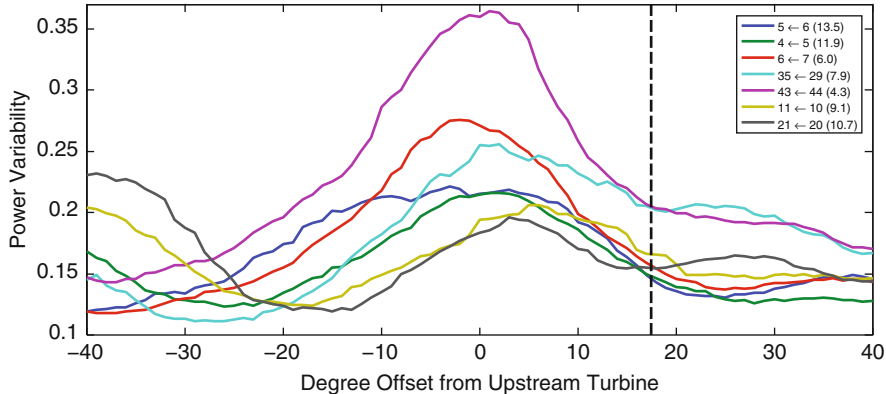


**Fig. 13.19** Power variability for shear speedup. As in Fig. 13.18, the  $x$ -axis gives the wind direction degree offset from the upwind turbine. The  $y$ -axis shows power variability

the increase occurs  $15^\circ$  to  $20^\circ$  from the bearing of the upstream turbine, with a magnitude of 1.1 to 1.22 times the average farm level. This magnitude is less than the speedup channel effect, but still significant. Again, this effect is associated with a wake presence. Effects like these have been observed in connection with buildings upstream to wind turbines (see, e.g., Corscadden et al. [20]). Building speedup is also seen in this data set (for example, turbine 7, bearing  $80^\circ$ ), but is not investigated further.

### ***Shear Speedup for Multiple Upstream Turbines***

Turbines 1, 6, 30, 31, 44, and 45 exhibit a narrow and a very high increase in performance close to due north. This is due to a displacement from multiple upstream turbines. Turbines 1 and 6 face a long row of turbines in an upstream wind farm at approximately  $15^\circ$ . The  $15^\circ$  angle is comparable to what is observed for the shear point speedup from a single turbine. Several other turbines, for example 7, 20, 29 and 43, also show the speedup, but the wake profiles are masked by a combination of speedup and wakening. The wake profiles for these turbines are shown in Figs. 13.20 and 13.21.

Turbines 44 and 45 are waked by a turbine and turbine 31 is facing multiple roughness elements. These three turbines show less performance increase than turbines 1, 6, and 30. All the turbines show a high variability towards the shear point to the left and slope down to an overall low of 0.12 to the right. The increase in power variability seen in Fig. 13.21 from  $25^\circ$  to  $40^\circ$  can be attributed to landscape roughness by farm buildings and clusters of tall trees.

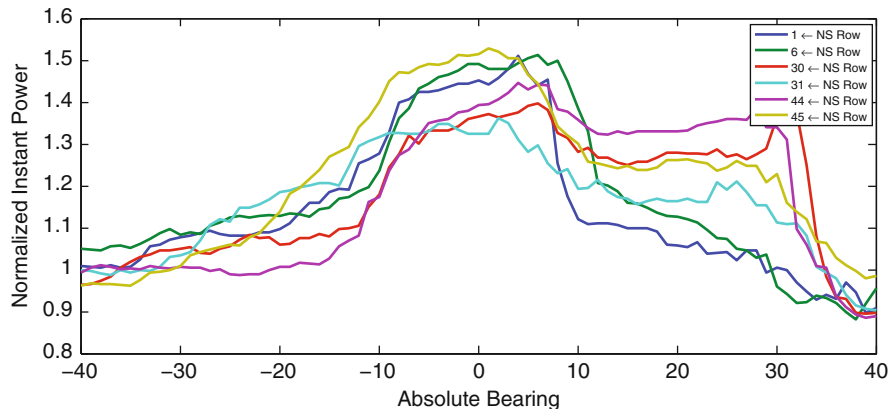


**Fig. 13.20** Normalized instant power increase from multiple upstream turbines. The normalized instant power profiles are shown for six turbines offset from an upstream row of turbines. The upstream turbine rows are all arranged from North to South

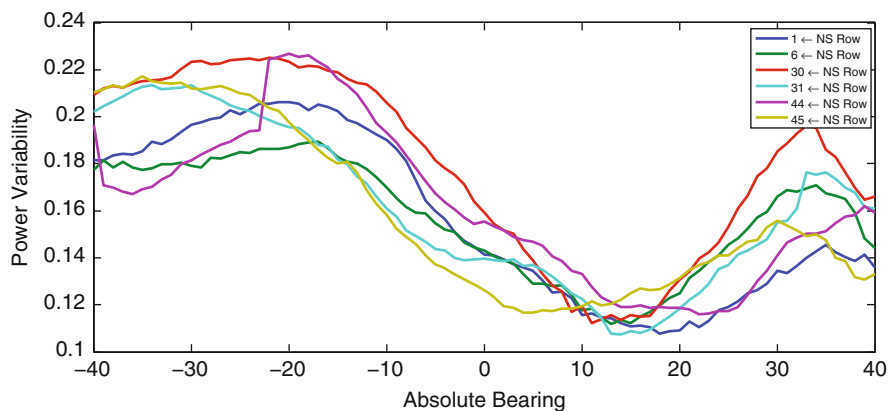


**Fig. 13.21** Power variability from multiple upstream turbines. The power variability profiles are shown for six turbines offset from an upstream row of turbines. The upstream turbine rows are arranged North to South

## References

1. J.F. Manwell, J.G. McGowan, A.L. Rogers, *Wind Energy Explained: Theory, Design and Application*, 2nd edn. (Wiley, 2009)
2. P.B.S. Lissaman, E.R. Bates, Energy effectiveness of arrays of wind energy conversion systems. Aerovironment Report AV FR 7050, Pasadena, CA, 1979
3. P.E.J. Vermeulen, An experimental analysis of wind turbine wakes, in *Proceedings of the Third International Symposium on Wind Energy Systems*, Lyngby, DK, 1980, pp. 431–450
4. I. Katic, J. Høstrup, N.O. Jensen, A simple model for cluster efficiency, in *Proceedings of the 1987 European Wind Energy Conference*, Rome, 1987, pp. 407–410

5. F. Gonzalez-Longatt, P. Wall, V. Terzija, Wake effect in wind farm performance: steady-state and dynamic behaviour. *Renew. Energy* **39**(1), 329–338 (2011). doi:[10.1016/j.renene.2011.08.053](https://doi.org/10.1016/j.renene.2011.08.053)
6. B. Sanderse, S.P. van der Pijl, B. Koren, Review of computational fluid dynamics for wind turbine wake aerodynamics. *Wind Energy* **14**, 799–819 (2011). doi:[10.1002/we.458](https://doi.org/10.1002/we.458)
7. R.J. Barthelmie, S.C. Pryor, S.T. Frandsen, K.S. Hansen, J.G. Schepers, K. Rados, W. Schlez, A. Neubert, L.E. Jensen, S. Neckelmann, Quantifying the impact of wind turbine wakes on power output at offshore wind farms. *J. Atmos. Oceanic Technol.* **27**, 1302–1317 (2010). doi:[10.1175/2010jtecha1398.1](https://doi.org/10.1175/2010jtecha1398.1)
8. F. Porte-Agel, Y.-T. Wu, C.-H. Chen, A numerical study of the effects of wind direction on turbine wakes and power losses in a large wind farm. *Energies* **6**, 5297–5313 (2013). doi:[10.3390/en6105297](https://doi.org/10.3390/en6105297)
9. A. Zaher, S.D.J. McArthur, D.G. Infield, Y. Patel, Online wind turbine fault detection through automated SCADA data analysis. *Wind Energy* **12**, 574–593 (2009). doi:[10.1002/we.319](https://doi.org/10.1002/we.319)
10. K. Kim, G. Parthasarathy, O. Uluyol, W. Foslien, S. Shuangwen, P. Fleming, Use of SCADA data for failure detection in wind turbines, in *Proceedings of 2011 Energy Sustainability Conference and Fuel Cell Conference*, 2011; NREL/CP-5000-51653
11. A. Kusiak, W. Li, The prediction and diagnosis of wind turbine faults. *Renew. Energy* **36**(1), 16–23 (2011). doi:[10.1016/j.renene.2010.05.014](https://doi.org/10.1016/j.renene.2010.05.014)
12. S. Butler, J. Ringwood, F. O'Connor, Exploiting SCADA system data for wind turbine performance monitoring, in *2013 Conference on Control and Fault-Tolerant Systems (SysTol)*, France, 2013, pp. 389–394. doi:[10.1109/systol.2013.6693951](https://doi.org/10.1109/systol.2013.6693951)
13. M. Schlechtingen, I.F. Santos, S. Achiche, Wind turbine condition monitoring based on SCADA data using normal behavior models. Part 1: system description. *Appl. Soft Comput.* **13**(1), 259–270 (2013). doi:[10.1016/j.asoc.2012.08.033](https://doi.org/10.1016/j.asoc.2012.08.033)
14. N.A. Johansen, *Verification of Simulated Fatigue Loads on Wind Turbines Operating in Wakes*, Master's Thesis, Technical University of Denmark, 2010
15. R.J. Barthelmie, L.E. Jensen, Evaluation of wind farm efficiency and wind turbine wakes at the Nysted offshore wind farm. *Wind Energy* **13**, 573–586 (2010)
16. K.S. Hansen, R.J. Barthelmie, L.E. Jensen, A. Sommer, The impact of turbulence intensity and atmospheric stability on power deficits due to wind turbine wakes at Horns Rev wind farm. *Wind Energy* **15**, 183–196 (2012)
17. N.G. Nygaard, Wakes in very large wind farms and the effect of neighboring wind farms. *J. Phys. The Science of Making Torque from Wind (TORQUE 2014)*
18. J.R. Marden, S.D. Ruben, L.Y. Pao, A model-free approach to wind farm control using game theoretic methods. *IEEE Trans. Control Syst. Technol.* **21**(4), 1207–1214 (2012)
19. C. Aggarwal, *Outlier Analysis* (Springer, New York, 2013)
20. K.W. Corscadden, W.D. Lubitzb, A. Thomson, J. McCabea, Investigation of wake effects on the energy production of small wind turbines. *Wind Eng.* **37**(2), 151–164 (2013). doi:[10.1260/0309-524x.37.2.151](https://doi.org/10.1260/0309-524x.37.2.151)
21. L.E. Jensen, Wake losses and turbulence within the horns rev off-shore wind farm, in *IEA Annex XXIII: Offshore Wind Energy Technology and Deployment, Task 23, Subtask 1, 3.1 Workshop Programme on External Conditions, Layouts, and Design of Off-Shore Wind Farms*, Risø, Denmark, 12–13 December 2005
22. P.E. Rethroe, N.A. Johansen, S.T. Frandsen, R.J. Barthelmie, K.S. Hansen, L.E. Jensen, M.A.B. Baekgaard, J.R. Kristoffersen, Systematic wind farm measurement data reinforcement tool for wake model calibration, in *European Offshore Wind Conference (EOW 2009)*